JMEPEG (2023) 32:2577–2586
https://doi.org/10.1007/s11665-022-06898-y

1059-9495/$19.00

TECHNICAL ARTICLE

Effect of Al-Ti Master Alloy on the Grain Refinement and Hot Tearing of AZ91 Mg Alloys

T.A. Davis and L. Bichler

Submitted: 16 December 2021 / Revised: 15 March 2022 / Accepted: 3 April 2022 / Published online: 25 April 2022

The AZ91D magnesium (Mg) alloy is a widely used aluminum (Al)-bearing commercial alloy. However, due to the presence of low-melting temperature phases, the alloy remains highly susceptible to hot tearing. In many Al and Mg alloys, grain refinement was seen to reduce the hot tearing severity, but an effective refiner for Al-bearing Mg alloys has been elusive. In the present work, a novel titanium (Ti)-based master alloy was developed using a spark plasma sintering (SPS) powder metallurgy route. Its effect on hot tearing was quantitatively studied in-situ using a mold with a load cell. In addition to a significant grain refinement, the master alloy eliminated hot tearing in casting conditions where untreated AZ91D Mg alloy readily nucleated hot tears.

Keywords advanced characterization, hot tearing, grain refinement, magnesium, titanium

1. Introduction

Magnesium (Mg) alloys containing a significant amount (>6 wt.%) of aluminum (Al), such as the AZ91D alloy, are extensively used in industrial applications due to their optimal strength, good castability and corrosion resistance. Wider adaptation of these alloys can be achieved if the room temperature mechanical performance can be further improved (Ref 1-4). Ex-situ grain refinement of Mg alloys is usually performed via master alloy addition. In the case of Al-containing Mg alloys, successful grain refinement has been limited, due to the interaction between the additives and the Al present in the Mg alloy, resulting in the formation of Al-rich secondary phases. For example, zirconium (Zr)-based refiners form an Al-Zr intermetallic, which poisons the grain refining effect in aluminum-bearing Mg alloys (Ref 2-4). Further, there remains a paucity of literature focusing on the interplay between grain refinement and casting defects in Al-containing Mg alloys (Ref 4-6).

In the case of Mg alloys, hot tearing remains an issue in casting of industrial parts with thin sections or complex 3D geometries (Ref 7-9). When hot tears nucleate near the end of a casting's solidification (fraction of solid > 0.9), a permanent crack typically forms in a casting region (on a macro-scale) under localized stress or strain (Ref 7, 9, 10). On the microstructure level, hot tears nucleate and propagate along the grain boundaries. The beneficial effect of grain refinement in combating hot tearing in aluminum alloys is well documented (Ref 9, 11-13), and grain refinement was seen to reduce the hot tearing susceptibility due to several proposed mechanisms, including: (1) ability of solid grains to slide past each other to accommodate thermal strain, (2) enhanced interdendritic feeding of liquid at high fraction of solids, (3) more homogeneous microstructure and dispersion of secondary phases, and (4) reduction and re-distribution of localized stress concentrations in the critical regions of the casting (Ref 14).

In this work, a novel master alloy containing two concentrations of titanium (Ti) in aluminum matrix was fabricated using the spark plasma sintering (SPS) powder metallurgy technique. The master alloys were successful in grain refining AZ91D Mg alloy. Further, the effect of the grain refinement on the evolution of hot tears was quantified using a mold, which enabled simultaneous in-situ analysis of solidification force and temperature. An in-depth microstructural characterization was carried out to study the interaction between the AZ91D alloy matrix and the Ti-based additives.

2. Experimental Procedure

2.1 Fabrication of Master Alloys Via SPS

Precursor high-purity Al powder (<45 μm particle size; Alfa Aesar #11067) and Ti powder (<45 μm particle size; Alfa Aesar #10386) were blended in a planetary ball mill (Fritsch Pulverisette 7). The resulting powder blend was then sintered using a Thermal Technologies 10-3 SPS machine with 20-mm graphite dies using proprietary sintering conditions (temperature, pressure and duration). Two master alloys were produced (defined by weight percent addition of Ti powder): (1) Al-6Ti, and (2) Al-18Ti.

This invited article is part of a special topical focus in the *Journal of Materials Engineering and Performance* on Magnesium. The issue was organized by Prof. C. (Ravi) Ravindran, Dr. Raja Roy, Mr. Payam Emadi, and Mr. Bernoulli Andilab, Ryerson University.

T.A. Davis and **L. Bichler**, School of Engineering, University of British Columbia – Okanagan, 3333 University Way, Kelowna V1V 1V7, Canada. Contact e-mail: lukas.bichler@ubc.ca.

2.2 Casting Procedure

A constrained rod casting mold (developed by Dr. N. Hort at the Magnesium Innovation Centre, Germany) with embedded load cell and thermocouples was used throughout this work. Prior studies with this mold are available in the literature (Ref 7, 15-18). As shown in Fig. 1, the geometry consisted of a vertical downsprue connected to a horizontal bar. The region joining the vertical downsprue and horizontal bar (i.e., 90° angle) induced a stress concentration in the casting, leading to the formation of hot tears. This area was labeled as the "critical region," since all hot tears consistently nucleated in this region. The repeatability, extent, and consistency of the hot tears have been confirmed by the authors (Ref 14, 19).

Previous studies by the authors with AZ91D Mg alloy revealed that a fixed pouring temperature of 720 °C and a mold temperature of 350 °C enabled fabrication of a tear-free casting. The onset of hot tearing (i.e., nucleation of micro-cracks) was observed when the mold temperature decreased to 325 °C. At 300 °C mold temperature, a visible macro hot tear formed. As a result, castings in this research were produced at the onset temperatures for hot tearing: 300 and 325 °C. Three replicates were produced at each mold temperature.

Table 1 lists the composition of the AZ91D Mg alloy used, as per the manufacturer specification sheet. The alloy had a slightly higher purity than generic AZ91 family of magnesium alloys.

Melt treatment with the master alloy was performed when the liquid alloy reached 740 °C. At this temperature, 0.1wt.% of the sintered master alloy was added and mechanically stirred (at 30 rpm, without breaking the metal surface) until dissolved. Following stirring, the melt was allowed to settle for 3 minutes, and then removed from the furnace and poured at 720 °C. Three compositions were studied at both mold temperatures based on the refinement addition: (1) Unrefined, (2) Low Ti (Al-6Ti), and (3) High Ti (Al-18Ti).

2.3 Data Analysis

Microstructural analysis of castings and master alloys was carried out with optical microscopy (OM) and scanning electron microscopy (SEM), while chemical analysis was performed with Oxford Aztec X-MAX XEDS. Acetic glycol etchant was used for OM characterization.

The as-cast grain size was measured using ASTM standard E112-13 via the Heyn linear intercept method (Ref 20). The line intercept pattern used was a combination of diagonal, vertical, and horizontal lines. This method has been successfully used by the authors earlier (Ref 19). The grain size was measured through the cross section of the critical hot tear region; the inset in Fig. 1 shows the location of these measurements as denoted by the red line. The average grain size reported in this work represents the grain size measurements in the core region of the critical region (i.e., ultrafine grains from the metal-mold interface region were not included in average grain size calculation).

The fraction of solid evolution (Eq 1) was calculated using the method proposed in Reference (Ref 21), where: f_s = fraction of solid, T_L = theoretical liquidus temperature of the alloy, T_S = theoretical solidus temperature of the alloy, and T = instantaneous temperature of the alloy. The authors have previously shown this formula has good alignment with in-situ measurement of the solidification of AZ91D Mg alloy (Ref 14, 22).

$$f_s = \frac{T_L - T + \frac{2}{\pi}(T_S - T_L)\left\{1 - \cos\left[\frac{\pi(T-T_L)}{2(T_S-T_L)}\right]\right\}}{(T_S - T_L)\left[1 - \frac{2}{\pi}\right]} \quad \text{(Eq 1)}$$

Vicker's microhardness was measured using a Wilson VH3300 automated tester, with a minimum of 30 indentations along the centerline of the horizontal bar in the critical hot tear region of each casting.

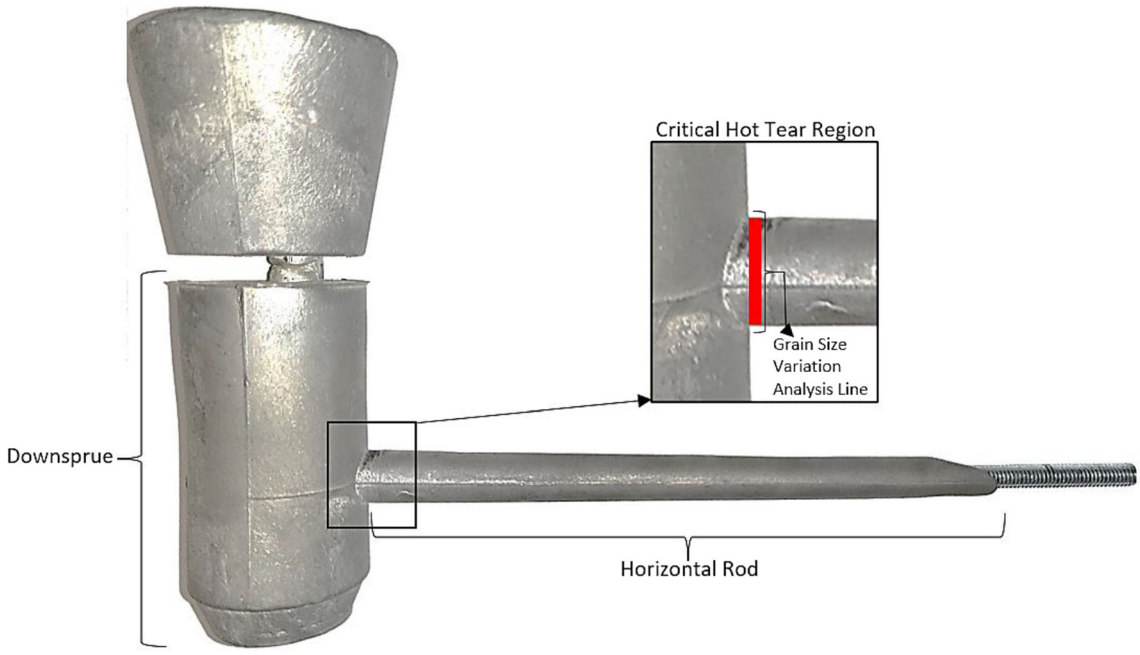

Fig. 1 Sample casting produced with the CRC mold. Critical hot tear region shown in inset

Table 1 AZ91D Mg alloy composition

Element	Al	Zn	Mn	Si	Cu	Fe	Be	Other	Mg
Composition (wt.%)	8.7	0.53	0.23	0.05	0.006	0.003	0.0012	0.3	Balance

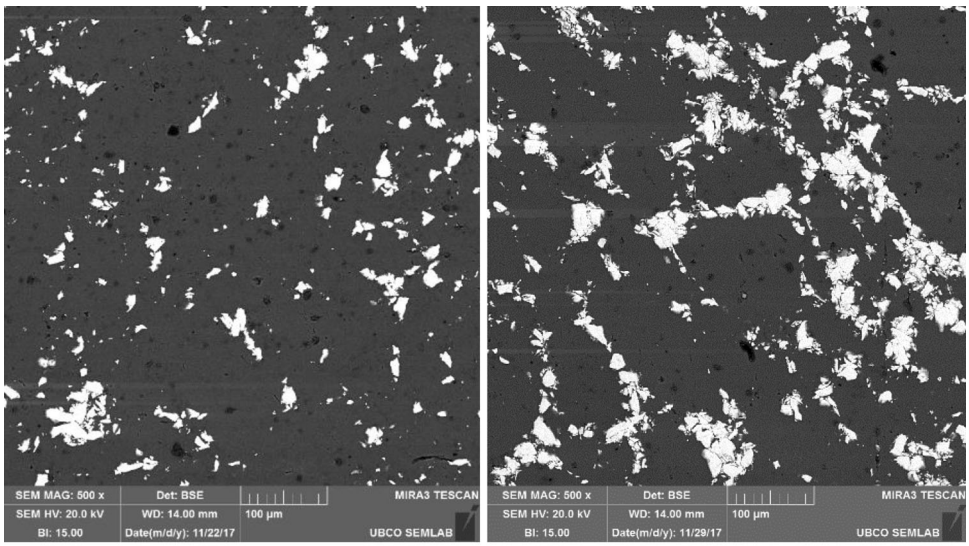

(a) (b)

Fig. 2 General microstructure of as-sintered: (a) Low Ti master alloy, (b) High Ti master alloy

3. Results and Discussion

3.1 General Microstructure of Master Alloys and Castings

Figure 2 shows the general microstructure of the as-sintered master alloys. During blending of the powders, Ti powder dispersion was achieved as a result of the high-energy milling process. As expected, the as-sintered master alloys contained the Ti particles along the grain boundaries of the Al matrix. In the case of the Low Ti master alloy, minimal agglomerations were observed, while in the case of the High Ti master alloy, the possibility of agglomeration of Ti particles along the grain boundaries has increased. Despite the increased volume fraction of the Ti particles along the grain boundaries in Fig. 2(b), the Ti particles remained separated and did not sinter to form large Ti aggregates.

During spark plasma sintering, consolidation is achieved via Joule heating between individual powder particles. In the case of electrically conductive Ti and Al powders used in this study, localized heating in the particle interface regions resulted in enhanced interdiffusion between the two constitutive powders. Figure 3 shows XEDS map and linescan results, indicating an evolution of an interfacial layer at the Ti-particle interfaces (for both Ti and Al). This interface between Ti and Al could be the $TiAl_3$ phase (Ref 23, 24), which has been reported to serve as an effective nucleant for Al alloys (Ref 25). Based on the planar disregistry between Mg and $TiAl_3$, this phase could serve as an effective nucleant for Mg and its alloys as well (Ref 26, 27). A similar evolution of an intermediate layer has been observed by the authors for other sintered refiners (Ref 19).

Figure 4 shows the general microstructure of the as-cast materials. The addition of the Al-Ti master alloys has resulted in a significant refinement of the grain structure at both mold temperatures, and also homogenized the dispersion of secondary phases. As shown in the etched micrographs, the $Mg_{17}Al_{12}$ (β)-phase was more uniformly dispersed and had a finer lamellar morphology than in an unrefined casting.

Figure 5 shows the measured average grain size of each alloy for both mold temperatures. The average reduction in grain size due to the Low Ti master alloy was ~75%, while the High Ti master alloy achieved ~78% reduction, at both mold temperatures. The master alloys have also significantly homogenized the grain size since the standard deviation in each refined casting significantly reduced as a result of refinement.

The variation of grain size throughout the cross section in the critical hot tearing region was examined. Figure 6 shows the grain size variation across the critical region of the horizontal bar. For both mold temperatures, the unrefined castings exhibited a large grain size increase in the center region of the horizontal bar, while the refined castings remained relatively uniform through the entire cross section. These results clearly illustrate the localized effect of the high heat transfer at the metal-mold interface, which enabled heterogeneous nucleation of the grains in the alloy, leading to a localized low grain size at the metal-mold interface (i.e., top skin or bottom skin regions). However, the unrefined casting exhibited a large grain size in the mid-section of the horizontal bar (i.e., center), indicating that grain growth was enabled by the relatively lower cooling rates. In the case of the refined castings, the grain size was uniform across the horizontal bar thickness, suggesting that the potency of the grain refiner was high, and surpassed the effect of the cooling rate on the grain size.

The structure of the Al-Ti inoculants after addition to the AZ91D alloy has been examined. Figure 7 shows a Ti-rich

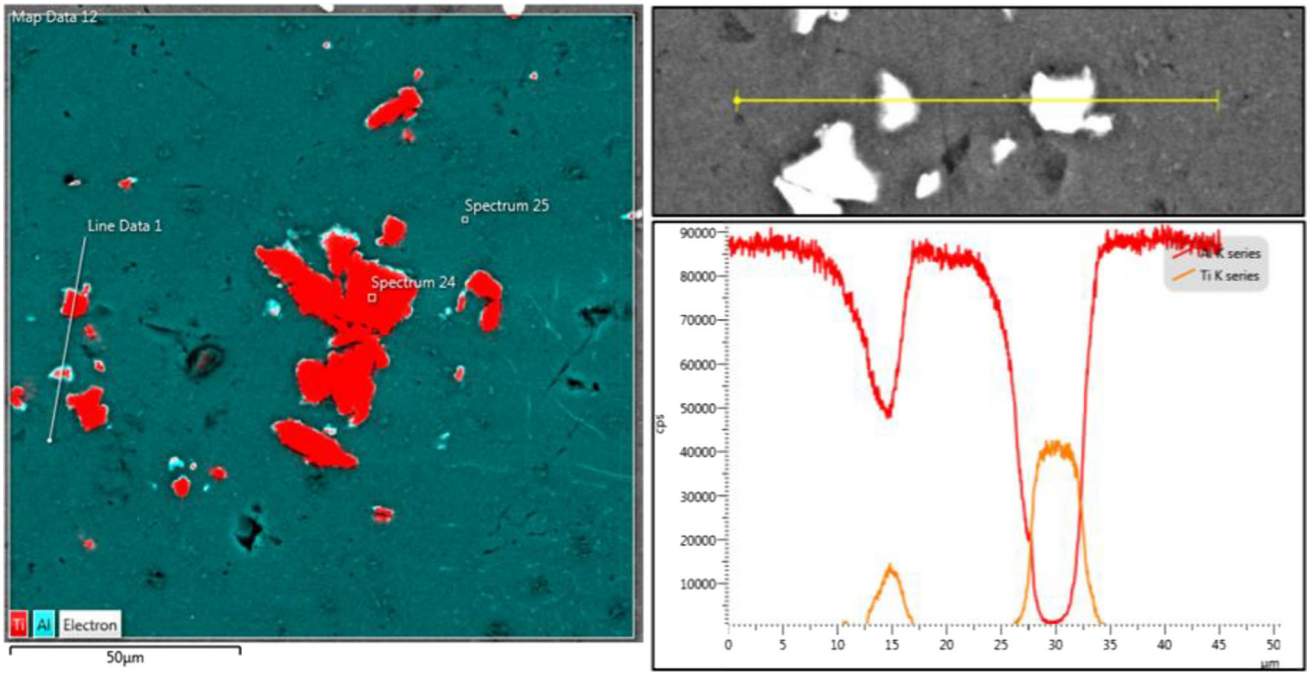

Fig. 3 SEM-XEDS characterization of particles in Low Ti master alloy

particle located in a grain interior in a casting produced with the High Ti grain refiner. The distribution of elements in the vicinity of the Ti-rich particle confirms that a transitional layer of Ti-Al-Mg has evolved in the as-cast material. The master alloy contained Al-Ti particles with a diffusion layer (originating from the SPS processing stage). In the as-cast material, the interdiffusion between the Ti-Al particle and surrounding Mg matrix is evident. As a result, it is likely that the particle was effectively wetted by the liquid alloy and possibly served as a heterogeneous nucleation site. Further, Ti has been suggested to contribute to grain refinement via grain growth restriction (Ref 6, 28, 29). Although some extent of Ti diffusion is evident in Fig. 7, it is likely that the primary mechanism of grain refinement was via heterogeneous nucleation.

3.2 Hot Tearing

Figure 8 shows micrographs from the 90 degree area of the casting (at the joining of the vertical downsprue and horizontal bar). In the case of the unrefined casting, a mold temperature decrease increased the alloy solidification rate, which resulted in a more pronounced hot tearing, as expected (Ref 7, 9, 21),

In the case of the unrefined casting produced at the 325 °C mold temperature, hot tearing was observed and the crack was mainly subsurface. This crack, however, was adjacent to significant shrinkage porosity, which has been suggested to act as a precursor for hot tear formation (Ref 9, 21). In the 300 °C mold temperature casting, a much wider and longer tear was observed, with the combined length of the tear nearly tripling.

Once the master alloys were added to the AZ91D alloy, nucleation and propagation of hot tears has significantly decreased (at both mold temperatures). At 325 °C mold temperature, the refined castings did not exhibit hot tears. At 300 °C mold temperature, hot tears spanning several grains were detected, but under all conditions remained significantly smaller than in the case of the unrefined castings.

The decrease in hot tearing with the addition of the grain refiner master alloys was likely also related to improved interdendritic feeding, which allowed enhanced compensation of evolving shrinkage porosity at high fractions of solid, thereby reducing thermal stresses developing in the as-cast material during solidification (Ref 17-19).

3.3 Force and Cooling Curves

The in-situ temperature and load data recorded during casting solidification are summarized in Table 2. The cooling rate and the force at the end of solidification for each mold temperature were quantified. Additionally, Fig. 9 shows the force and temperature curves for the 325 and 300 °C mold temperature casting, respectively.

Table 2 shows that the increase in hot tearing severity in the unrefined castings was related to the increased solidification rate and the increased force development at the end of solidification. Conversely, with the addition of both Al-Ti master alloys, an increased solidification rate was observed without an increase in force development at the end of solidification.

As seen in Fig. 9, the unrefined castings exhibited force variations (jogs in the curve) during solidification, which corresponded with hot tear nucleation and/or propagation. Notably there was a large slope change recorded in all force curves at $\sim$ 10-20 seconds into solidification, at which point the fraction of solid was $>$ 0.9.

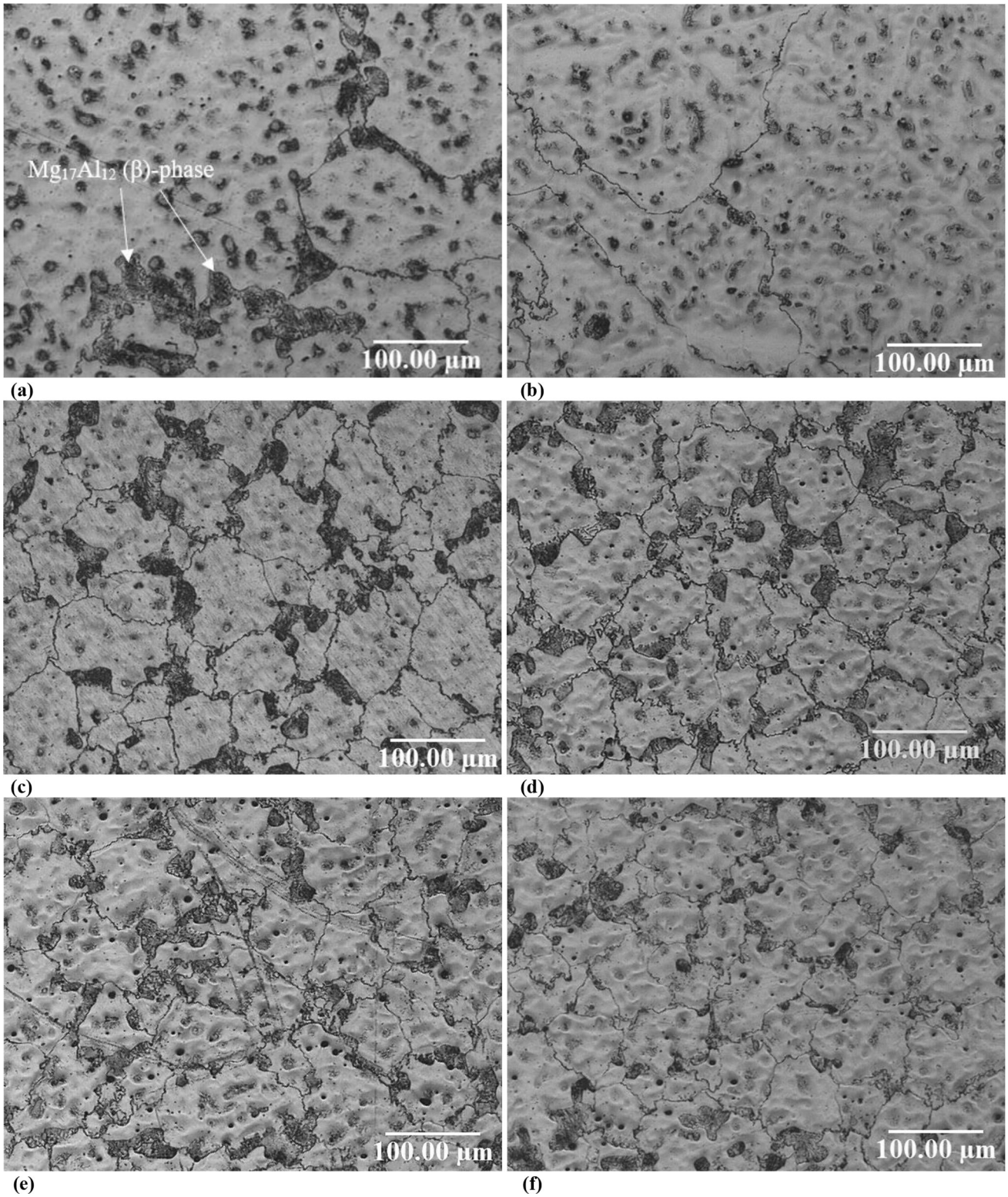

Fig. 4 As-cast microstructure of alloys (treatment and mold temperature): (a) Unrefined 325 °C, (b) Unrefined 300 °C, (c) Low Ti 325 °C, (d) High Ti 325 °C, (e) Low Ti 300 °C, (f) High Ti 300 °C

Both Al-Ti master alloys exhibited consistent cooling curves suggesting that an increase in Ti content did not significantly change the solidification kinetics once alpha-Mg nucleated. A marginal variation in the cooling curves was observed when the casting temperature reached ~500-525 °C, which corresponded to ~0.85-0.9 fraction of solid. The shape of the cooling curves observed in this research is consistent with literature (Ref 7, 17, 19).

Figure 10 shows the fraction of solid evolution in relation to the force experienced by the casting. From this data, the observed reduction in hot tearing can be related to the strain (and stress) evolved in the casting during solidification. At both mold temperatures, the force in the refined castings developed at a later stage of solidification ($>$ 0.8 fraction of solid). This suggests that when the grain refined castings reached a critical stage of solidification with regards to hot tearing, a lower force evolved on the coherent dendritic structure compared to the unrefined castings.

3.4 Mechanical Hardness

Figure 11 summarizes the Vicker's microhardness values of the various castings produced at different mold temperatures. The hardness of the unrefined AZ91D Mg alloy was consistent with literature for permanent-mold cast as-cast materials (Ref 5, 28). On average, the hardness increased by ~15% with the addition of the master alloys. The hardness increase has been attributed to a more homogenous grain structure and a grain size reduction causing an increased grain boundary area (Ref 5, 28).

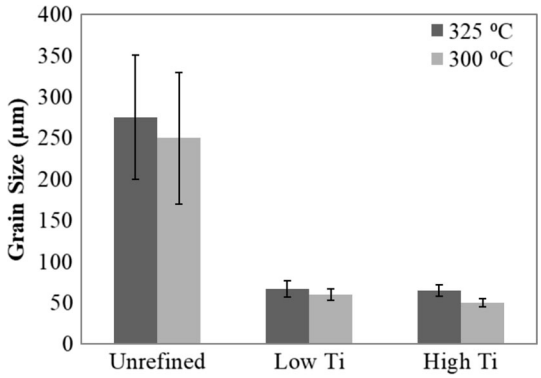

Fig. 5 Average grain size of castings at each mold temperature and refinement level

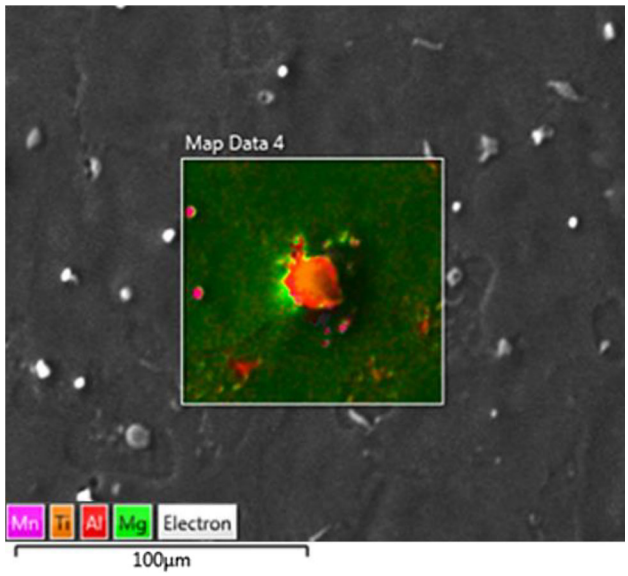

Fig. 7 Al-Ti particle in a casting produced with High Ti master alloy and 325 °C mold temperature

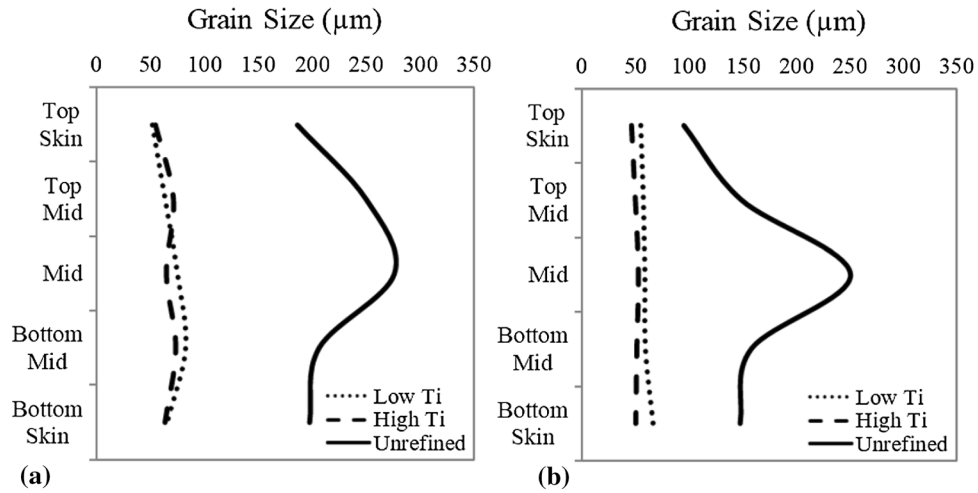

Fig. 6 Grain size variation through cross section of the critical hot tear region of: (a) 325 °C and (b) 300 °C mold temperature castings

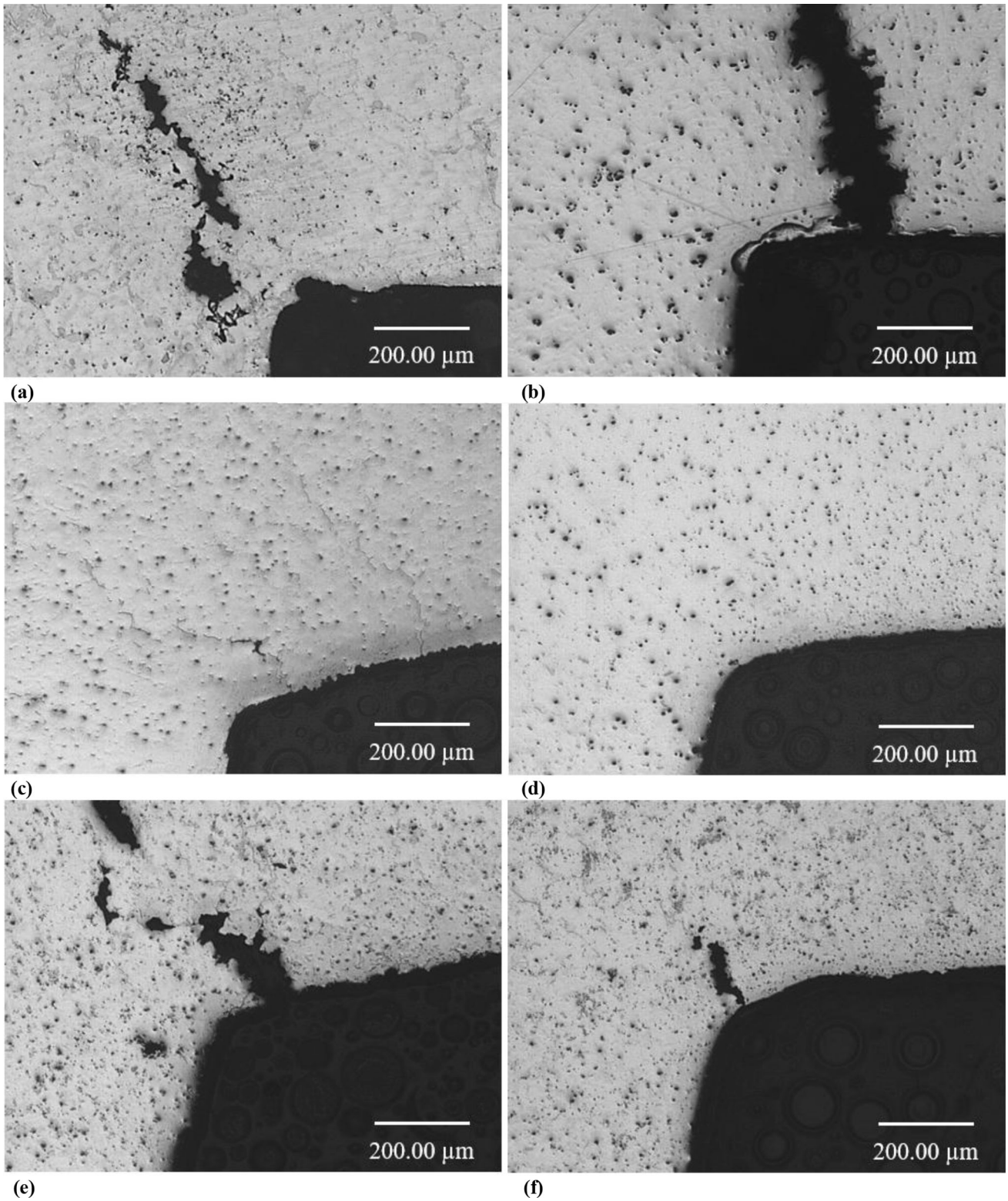

Fig. 8 Micrographs of hot tear severity for each casting at 100x magnification (treatment and mold temperature): (a) Unrefined 325 °C, (b) Unrefined 300 °C, (c) Low Ti 325 °C, (d) High Ti 325 °C, (e) Low Ti 300 °C, (f) High Ti 300 °C

Table 2 Cooling rate and force of castings produced with different mold temperatures and refinement levels

	Cooling Rate, °C/s)		End of Solidification Force, N	
	325 °C	300 °C	325 °C	300 °C
Unrefined	1.6 ± 0.15	3.2 ± 0.2	70 ± 4	90 ± 5
Low Ti	2.6 ± 0.1	4.4 ± 0.15	50 ± 2	50 ± 2
High Ti	2.4 ± 0.1	4.4 ± 0.2	50 ± 1	57 ± 3

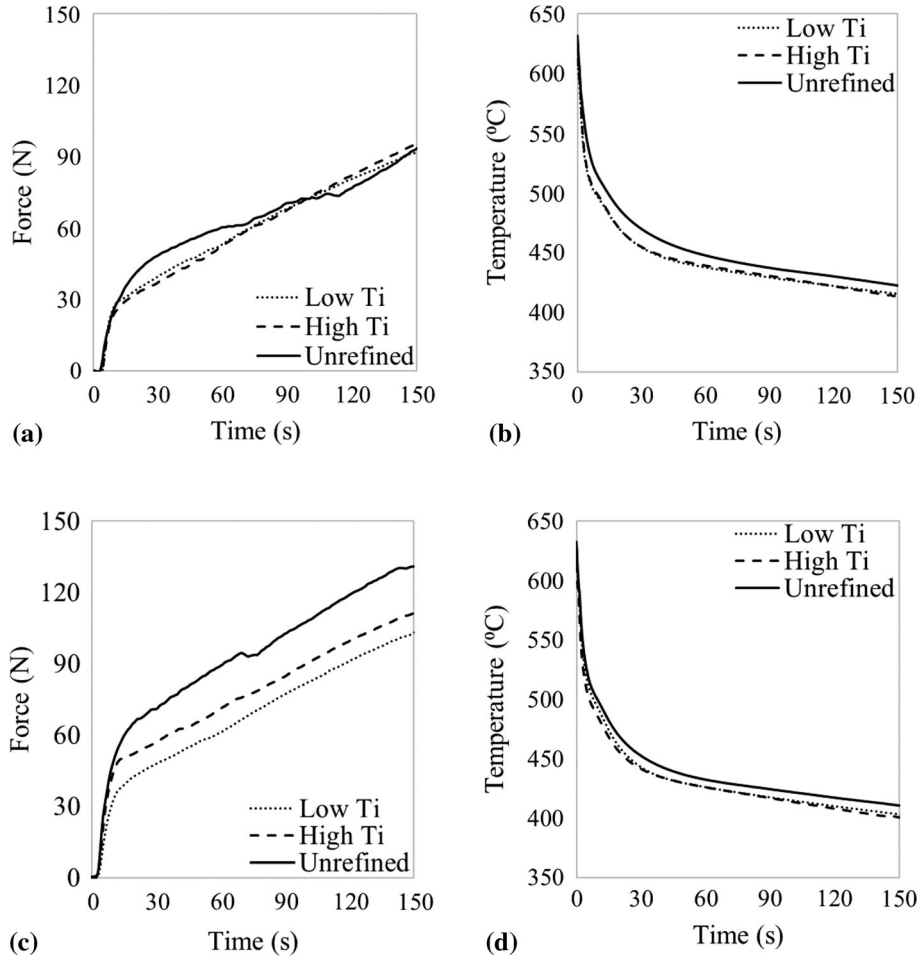

Fig. 9 Force and cooling curves for castings produced at different mold temperatures: (a) 325 °C force curves, (b) 325 °C cooling curves, (c) 300 °C force curves, (d) 300 °C cooling curves

4. Conclusions

Analysis of a novel Al-Ti master alloy for grain refinement of an aluminum bearing Mg alloy has been presented. The following conclusions from this research have been drawn.

1. Using the spark plasma sintering (SPS) approach, two novel Al-Ti master alloys have been developed and used to effectively grain refine AZ91D Mg alloy.
2. Detailed analysis of the master alloys revealed that the SPS process enabled chemical reactions between the Ti and Al powders.
3. Hot tearing has been significantly reduced in conditions where it was prevalent in unrefined AZ91D Mg alloy. Comparison of the cooling data with the force evolution has shown that the addition of the master alloy lowered the magnitude of force evolving in the dendritic structure during solidification.

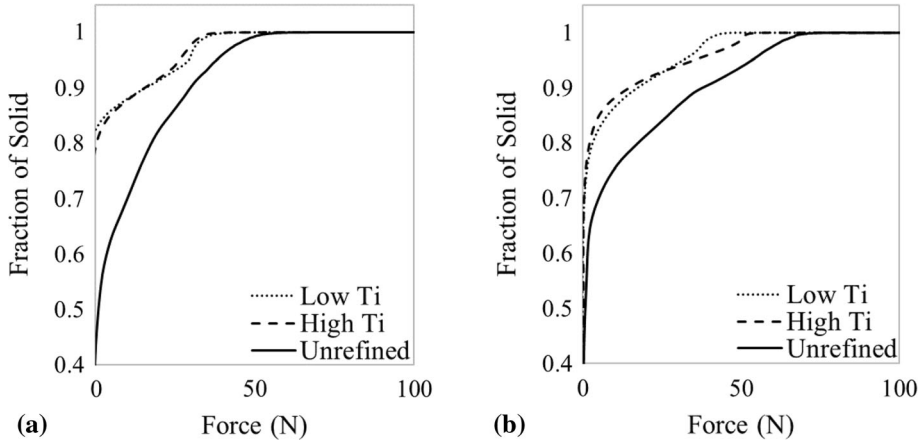

Fig. 10 Fraction of solid vs. force curves for (a) 325 °C and (b) 300 °C mold temperature castings

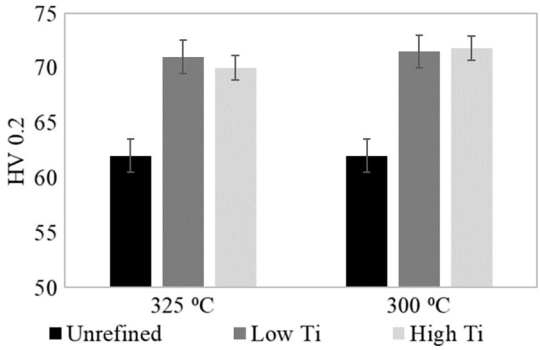

Fig. 11 Average microhardness of castings for each mold temperature and refinement level

Acknowledgments

The authors would like to acknowledge the financial support from NSERC and the NSERC Discovery Grant. The authors would also like to acknowledge the support from Dr. Norbert Hort and the Magnesium Innovation Centre located at Helmholtz-Zentrum in Geesthacht, Germany.

References

1. M.A. Easton, M. Qian, A. Prasad, and D.H. StJohn, Recent Advances in Grain Refinement of Light Metals and Alloys, *Curr. Opin. Solid State Mater. Sci.*, 2016, **20**(1), p 13–24. https://doi.org/10.1016/j.cossms.2015.10.001
2. T.J. Chen, X.D. Jiang, Y. Ma, Y.D. Li, and Y. Hao, Grain Refinement of AZ91D Magnesium Alloy by SiC, *J. Alloy. Compd.*, 2010, **496**(1–2), p 218–225. https://doi.org/10.1016/j.jallcom.2010.03.002
3. Y. Ali, D. Qiu, B. Jiang, F. Pan, and M.X. Zhang, Current Research Progress in Grain Refinement of Cast Magnesium Alloys: A Review Article, *J. Alloy. Compd.*, 2015, **619**, p 639–651. https://doi.org/10.1016/j.jallcom.2014.09.061
4. D.H. StJohn, M.A. Easton, M. Qian, and J.A. Taylor, Grain Refinement of Magnesium Alloys: A Review of Recent Research, Theoretical Developments, and Their Application, *Metall. and Mater. Trans. A.*, 2013, **44**(7), p 2935–2949. https://doi.org/10.1007/s11661-012-1513-x
5. T.J. Chen, R.Q. Wang, Y. Ma, and Y. Hao, Grain Refinement of AZ91D Magnesium Alloy by Al-Ti-B Master Alloy and its Effect on Mechanical Properties, *Mater. Des.*, 2012, **34**, p 637–648. https://doi.org/10.1016/j.matdes.2011.05.020
6. M. Vlasceanu, S. Lun Sin, A. Elsayed, and C. Ravindran, Effect of Al–5Ti–1B on Grain Refinement, Dendrite Coherency and Porosity of AZ91E Magnesium Alloy, *Int. J. Cast Metals Res.*, 2015, **28**(1), p 39–46
7. Z.S. Zhen, N. Hort, Y.D. Huang, O. Utke, N. Petri, and K.U. Kainer, Hot Tearing Behaviour of Binary Mg-1Al alloy Using a Contraction Force Measuring Method, *Int. J. Cast Met. Res.*, 2009, **22**(1–4), p 331–334. https://doi.org/10.1179/136404609X368145
8. A. Elsayed, C. Ravindran, and B.S. Murty, Effect of Al-Ti-B Based Master Alloys on Grain Refinement and Hot Tearing Susceptibility of AZ91E Magnesium Alloy, *Mater. Sci. Forum*, 2011, **690**, p 351–354. https://doi.org/10.4028/www.scientific.net/MSF.690.351
9. J. Song, F. Pan, B. Jiang, A. Atrens, M.X. Zhang, and Y. Lu, A Review on Hot Tearing of Magnesium Alloys, *J. Magn. Alloys*, 2016, **4**(3), p 151–172. https://doi.org/10.1016/j.jma.2016.08.003
10. Y. Wang, B. Sun, Q. Wang, Y. Zhu, and W. Ding, An Understanding of the Hot Tearing Mechanism in AZ91 Magnesium Alloy, *Mater. Lett.*, 2002, **53**(1–2), p 35–39. https://doi.org/10.1016/S0167-577X(01)00449-9
11. S. Li, and D. Apelian, Hot Tearing of Aluminum Alloys a Critical Literature Review, *Int. J. Metalcast.*, 2011, **5**(1), p 23–40
12. D.G. Eskin, Suyitno and L. Katgerman, Mechanical Properties in the Semi-Solid State and Hot Tearing of Aluminium Alloys, *Prog. Mater. Sci.*, 2004, **49**(5), p 629–711
13. C. Davidson, D. Viano, L. Lu and D. StJohn, Observation of Crack Initiation During Hot Tearing, *Int. J. Cast Met. Res.*, 2006, **19**(1), p 59–65. https://doi.org/10.1179/136404606225023291
14. T.A. Davis, Development of Novel Grain Refiners for AZ91D Magnesium Alloys and Their Effect on Hot Tearing, *Univ. Br. Columbia*, 2019. https://dx.doi.org/10.14288/1.0378555
15. Z. Wang et al., Experimental and Numerical Analysis of Hot Tearing Susceptibility for Mg-Y Alloys, *J. Mater. Sci.*, 2014, **49**(1), p 353–362. https://doi.org/10.1007/s10853-013-7712-z
16. Z. Wang et al., Hot Tearing Susceptibility of Binary Mg-Y Alloy Castings, *Mater. Des.*, 2013 https://doi.org/10.1016/j.matdes.2012.12.044
17. L. Zhou, Y.-D. Huang, P.-L. Mao, K.U. Kainer, Z. Liu and N. Hort, Influence of Composition on Hot Tearing in Binary mg-zn Alloys, *Int. J. Cast Met. Res.*, 2011, **24**(3–4), p 170–176. https://doi.org/10.1179/136404611X13001912813942
18. Z. Liu, S.B. Zhang, P.L. Mao and F. Wang, Effects of Y on Hot Tearing Formation Mechanism of Mg-Zn-Y-Zr Alloys, *Trans. Nonferrous Metals Soc. China (English Edition)*, 2014, **24**(4), p 907–914. https://doi.org/10.1016/S1003-6326(14)63142-3
19. T.A. Davis, L. Bichler, F. D'Elia and N. Hort, Effect of TiBor on the Grain Refinement and Hot Tearing Susceptibility of AZ91D magnesium Alloy, *J. Alloy. Compd.*, 2018, **759**, p 70–79. https://doi.org/10.1016/j.jallcom.2018.05.129
20. ASTM, E112-13: Standard test methods for determining average grain size, West Conshohocken, PA, 2013
21. L. Bichler, C. Ravindran and D. Sediako, Onset of Hot Tearing in AE42 Magnesium Alloy, *Can. Metall. Q.*, 2009, **48**(1), p 81–89. https://doi.org/10.1179/000844309794239170

22. T.A. Davis, L. Bichler, D. Sediako and L. Balogh, Solidification Analysis of Grain Refined AZ91D Magnesium Alloy via Neutron Diffraction, *Magnesium Technology*, 2018, **2018**, p 425–428. https://doi.org/10.1007/978-3-319-72332-7_65
23. P.S. Mohanty and J.E. Gruzleski, Grain Refinement of Aluminium by TiC, *Scripta Metallurgica et Materiala*, 1994, **31**(2), p 179–184. https://doi.org/10.1016/0956-716X(94)90171-6
24. Z.W. Liu, M. Rakita, Q. Han and J.G. Li, A Developed Method for Fabricating in-situ ticp /mg Composites by Using Quick Preheating Treatment and Ultrasonic Vibration, *Metall. Mater. Trans. A*, 2012, **43**(6), p 2116–2124. https://doi.org/10.1007/s11661-011-1041-0
25. J. Wang et al., Microstructural Evolution and Grain Refining Efficiency of Al-10Ti Master Alloy Improved by Copper Mold Die Casting, *J. Mater. Eng. Perform.*, 2013, **22**(7), p 2012–2018. https://doi.org/10.1007/s11665-013-0490-6
26. Y. Watanabe, Y.B. Gao, J.Q. Guo, H. Sato, S. Miura and H. Miura, Heterogeneous Nucleation of Pure Magnesium on Al 3 Ti, TiC, TiB 2, and AlB 2 Particles, *Jpn. J. Appl. Phys.*, 2013, **52**(1S), p 01AN04
27. A. Elsayed, Inclusion Removal and Grain Refinement of Magnesium Alloy Castings, Ryerson University, 2015
28. J. Chen, Y. Sun, J. Zhang, W. Cheng, X. Niu and C. Xu, Effects of Ti Addition on the Microstructure and Mechanical Properties of Mg-Zn-Zr-Ca Alloys, *J. Magn. Alloys*, 2015, **3**(2), p 121–126. https://doi.org/10.1016/j.jma.2015.05.001
29. Y. Wang, X. Zeng, W. Ding, A. Luo and A.K. Sachdev, Grain Refinement of AZ31 Magnesium Alloy by Titanium and Low-Frequency Electromagnetic Casting, *Metall. and Mater. Trans. A.*, 2007, **38**(6), p 1358–1366. https://doi.org/10.1007/s11661-007-9215-5